



HAL
open science

A new strategy to prepare alumina-zirconia composite or multilayered coatings by combining cold-spray deposition and plasma electrolytic oxidation

J. Martin, A. Maizeray, C. da Silva Tusch, G. Marcos, T. Czerwiec, G. Henrion

► To cite this version:

J. Martin, A. Maizeray, C. da Silva Tusch, G. Marcos, T. Czerwiec, et al.. A new strategy to prepare alumina-zirconia composite or multilayered coatings by combining cold-spray deposition and plasma electrolytic oxidation. *Materials Today Communications*, 2023, 36, pp.106676. 10.1016/j.mtcomm.2023.106676 . hal-04164070

HAL Id: hal-04164070

<https://hal.science/hal-04164070>

Submitted on 18 Jul 2023

HAL is a multi-disciplinary open access archive for the deposit and dissemination of scientific research documents, whether they are published or not. The documents may come from teaching and research institutions in France or abroad, or from public or private research centers.

L'archive ouverte pluridisciplinaire **HAL**, est destinée au dépôt et à la diffusion de documents scientifiques de niveau recherche, publiés ou non, émanant des établissements d'enseignement et de recherche français ou étrangers, des laboratoires publics ou privés.

**A new strategy to prepare alumina-zirconia composite or multilayered coatings by
combining cold-spray deposition and plasma electrolytic oxidation**

J. Martin^{1,2*}, A. Maizeray^{1,2}, C. Da Silva Tusch¹, G. Marcos^{1,2}, T. Czerwicz^{1,2}, G. Henrion^{1,2}

¹ Université de Lorraine, CNRS, IJL, F-54000 Nancy, France

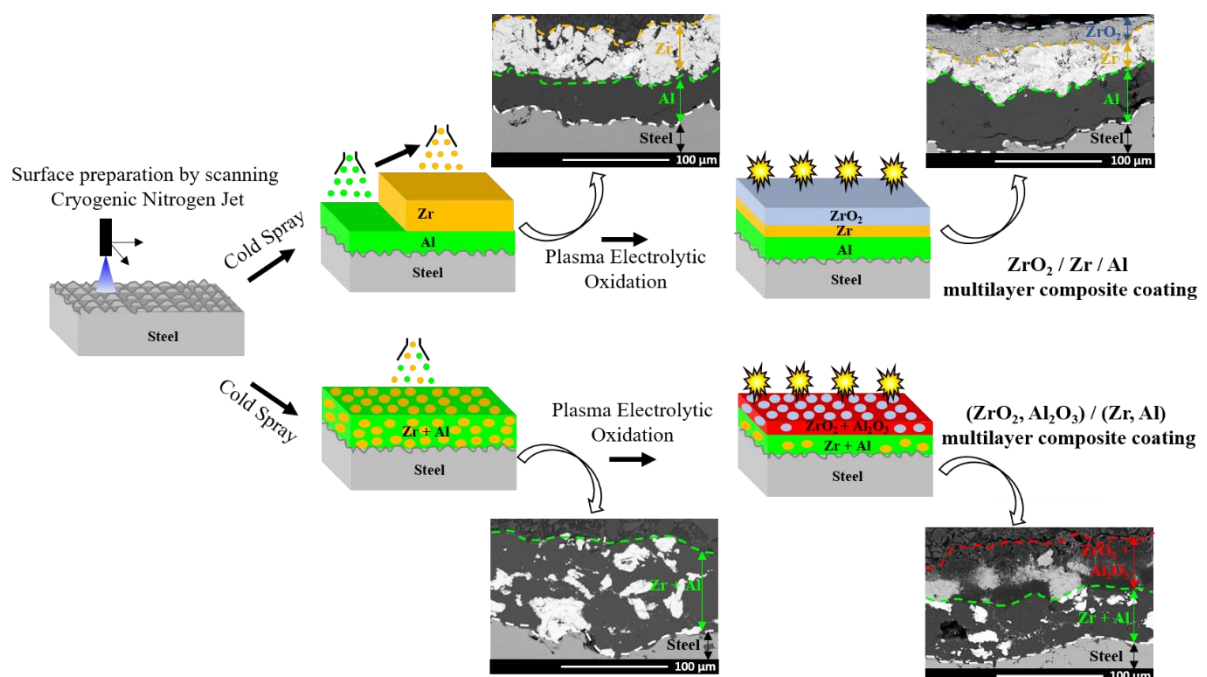
² Université de Lorraine, Laboratoire d'Excellence Design of Alloy Metals for low-mAss Structures ('LabEx DAMAS'), F-57045 Metz, France

*Corresponding author: +33 (0)3.72.74.24.97, julien.martin@univ-lorraine.fr

Highlights

- A Zr / Al metallic multilayer coating was successfully cold-sprayed on steel.
- After oxidation by PEO, a ZrO_2 / Zr / Al composite multilayer coating was produced.
- A (Zr, Al) metallic monolayer coating was successfully cold-sprayed on steel.
- After oxidation by PEO, a $(\text{ZrO}_2, \text{Al}_2\text{O}_3)$ / (Zr, Al) composite multilayer coating was produced.

Graphical abstract



Abstract

In the present study, the feasibility of the elaboration of alumina (Al_2O_3) - zirconia (ZrO_2) composite coatings on steel was explored by combining cold-spray deposition and plasma electrolytic oxidation (PEO). More specifically, two different configurations were investigated. The first configuration consisted in successively cold-spraying an aluminium layer first and a zirconium layer second, giving rise to a Zr / Al metallic multilayer coating that was then partially oxidized by PEO. In this configuration, microstructural characterizations evidenced the formation of a ZrO_2 / Zr / Al composite multilayer coating on steel. The second configuration consisted in simultaneously cold-spraying aluminium and zirconium into a (Zr, Al) metallic composite monolayer prior to its partial oxidation by PEO. In this case, results evidenced the formation of a $(\text{ZrO}_2, \text{Al}_2\text{O}_3)$ / (Zr, Al) composite multilayer coating on steel. Finally, the present study demonstrated that the duplex surface treatment combining cold-spray deposition and PEO method is viable as a new route to produce ceramic/metal composite coatings on various metallic alloys.

Keywords: Duplex treatment; Cold-spray deposition; Plasma electrolytic oxidation (PEO); Ceramic/metal composite coating; Zirconia; Alumina

1. Introduction

Steels are the most used metallic alloys in various domains, mainly due to their attractive mechanical properties such as high tensile strength, high toughness, and good machining ability, combined with a low processing cost. Nevertheless, steels suffer from their weak resistance against corrosion, thus restricting their use in many corrosive environments, including hot oxidizing gases and oils, biological media and irradiating environments [1]. Even if stainless steels have shown better high-temperature resistance against corrosive media, their surface hardness and their wear resistance remains too low in severe service conditions. To increase the service life of steel components, key strategies are generally centered on surface engineering with the aim of carefully modifying the surface microstructure and composition without sacrificing the mechanical properties of the bulk material [2, 3].

Surface treatments mostly focus on the formation of hard and protective ceramic coatings that usually consist of Al_2O_3 [4-6]. Indeed, alumina is considered as a material of choice for surface protection of metals since this ceramic exhibits a high hardness, a high chemical stability, a low corrosion rate in harsh environments and an extremely low oxygen diffusion rate [7-9]. An effective approach to further enhance the protective performance of alumina consists in mixing it with complementary ceramic materials such as MoO_2 , ZrO_2 , SiC , TiO_2 or SiO_2 [10-15]. Among the alumina-based composites, Al_2O_3 - ZrO_2 system has demonstrated unique features to achieve synergetic protective properties [16]. Indeed, due to the insolubility of zirconia in alumina over a wide range of temperature, Al_2O_3 - ZrO_2 ceramic compounds can form and have the potential to combine the high hardness and high chemical inertness of alumina with the excellent toughness of zirconia [17, 18]. Thus, the advanced Al_2O_3 - ZrO_2 composite ceramic coatings on metal substrates are widely used for their excellent corrosion resistance [19-21], their high friction and wear resistance [22, 23], their improved mechanical

resistance even at high temperature (high fracture toughness and high thermal-shock resistance) [24-26] as well as their good biocompatibility [27, 28]. Nowadays, alumina-zirconia ceramics have attracted significant attention in many fields such as cutting tools, bearings, hip prostheses and dental implants [28, 29] or even thermal barrier coatings (TBCs) for hot section components of engines [30, 31]. In recent years, many techniques have been used to synthesize $\text{Al}_2\text{O}_3\text{-ZrO}_2$ composite coatings with varying morphologies and compositions, such as physical vapor deposition (PVD) [32, 33], chemical vapor deposition (CVD) [34], atmospheric plasma spray (APS) [35, 36], high velocity oxy fuel (HVOF) [18], spark plasma sintering [37] and sol-gel [38, 39]. However, the coatings formed by these techniques are usually thin (between 100 nm and 5 μm) and/or have relatively low adhesion strength [40]. They are also usually amorphous and a subsequent heat treatment at relatively high temperature is required to crystallize the coatings, which can cause the delamination of the coating from the metallic substrate [41].

Plasma electrolytic oxidation (PEO), also called micro-arc oxidation (MAO), is a plasma-assisted electrochemical coating technique that can produce thick, crystalline and well-adherent protective oxide coatings on the surface of valve metals like aluminium, titanium, magnesium and their alloys [42-46] while using environmental friendly electrolytes. Depending on the base metal treated, ceramic PEO coatings exhibit enhanced performances in terms of wear [47], corrosion [48, 49] and thermal resistance [50-52], biocompatibility [53, 54], and photocatalytic properties [55, 56]. PEO process parameters, especially the electrical conditions applied to the electrodes and the chemical composition of the electrolyte control the thermal, electrochemical, and plasma phase reactions that take place locally on the processed surface [57-62]. In the specific case of the PEO of aluminium, it is well-established that these parameters directly influence the grown alumina coating in terms of microstructure, porosity, thickness, crystallography, elemental composition, etc.

Many studies report on the possible elaboration of Al₂O₃-ZrO₂ composite coatings by PEO [63-78]. However, the main strategy in all these works consists in modifying the electrolyte, either by dispersing micro- or nano-ZrO₂ particles [63-66] or by dissolving zirconium-based salts (K₂ZrF₆, ZrOCl₂, Zr(OH)₄) [67-72]. In the former case, the formation of the Al₂O₃-ZrO₂ composite coating occurs by the electrophoretic penetration of the dispersed ZrO₂ particles into the growing Al₂O₃ PEO coating [10, 73, 74]. In the second case, its formation proceeds by the plasma-assisted electrochemical reactions that take place between the dissolved chemical species, involving complexation of zirconium ions, and their precipitation into zirconia through the growing Al₂O₃ PEO coating [68, 75, 76]. However, in most cases, the preparation of Al₂O₃-ZrO₂ composite coatings by modifying the PEO electrolyte faces limiting factors due to a low and an uncontrolled incorporation rate as well as a heterogeneous distribution of ZrO₂ and Al₂O₃ throughout the thickness of the PEO coatings, the outer sublayer being preferentially enriched with ZrO₂ ceramic [77]. Moreover, the PEO process remains strictly inoperative on non-valve metals like steels [46, 78].

Combining cold spray deposition (CS) with plasma electrolytic oxidation can advantageously overcome these limitations, and make it possible to elaborate Al₂O₃ / ZrO₂ composite coatings on non-valve metals, while keeping the main advantages of the PEO process. Based on recent results [79], the present study aims at exploring the feasibility of growing (Al₂O₃, ZrO₂)-based composite coatings on steel by a duplex process within two different configurations of CS and PEO. A first one consisted in producing a ZrO₂ / Zr / Al multilayer composite coating with the aim of replicating the typical arrangement of thermal barrier coatings (TBCs) [30, 31]. The second configuration consisted in developing a (Al₂O₃-ZrO₂) monolayer composite coating that may potentially find applications in many fields such as cutting tools, bearings and biomaterials for orthopedic implants [19, 22, 24, 27]. The

evaluation of the functional properties of the produced coatings will be the subject of further studies.

2. Materials and Methods

Commercial S235 steel (table 1) was used as metallic substrate. The samples exhibited a rectangular shape of $40 \times 30 \times 6 \text{ mm}^3$ with a processed surface area of about 12 cm^2 . As depicted in figure 1, and prior to be cold-sprayed, surfaces were prepared by high pressure ($\sim 3000 \text{ bars}$) and low temperature ($\sim -170 \text{ }^\circ\text{C}$) cryogenic nitrogen jet [80]. It provided a significant roughness ($R_a = 45 \text{ } \mu\text{m} \pm 5 \text{ } \mu\text{m}$) ensuring good adhesion of the cold-sprayed coating to the steel substrate.

Commercial 1050 grade aluminium (table 2) and commercially pure zirconium metallic powders (table 3) were cold-sprayed on the steel substrate. The aluminium powder consisted of spherical Al particles with an average diameter of $36 \text{ } \mu\text{m} \pm 3 \text{ } \mu\text{m}$. The zirconium particles also exhibited a spherical shape with an average diameter of $42 \text{ } \mu\text{m} \pm 6 \text{ } \mu\text{m}$. Cold-sprayed coatings were prepared by using nitrogen as carrier gas with pressure and temperature parameters set to 25 bars and $340 \text{ }^\circ\text{C}$, respectively. The spray-angle was 90° and the nozzle was set at 30 mm from the substrate.

Fig. 1 depicts the two configurations of the duplex treatment that were carried out in order to produce two sets of $(\text{ZrO}_2, \text{Al}_2\text{O}_3) / (\text{Zr}, \text{Al})$ composite multilayer coatings. The first configuration was obtained by successively cold-spraying an aluminium layer on the steel substrate, and a zirconium layer on top of the cold-sprayed aluminium. The resulting Zr / Al metallic multilayer coating was then PEO-processed to elaborate a $\text{ZrO}_2 / \text{Zr} / \text{Al}$ composite

multilayer coating. The second configuration consisted in simultaneously cold-spraying aluminium and zirconium powders in equal volume proportion on the steel substrate. Co-spraying was achieved using two powder tanks, each containing one metallic powder. The resulting (Zr, Al) metallic monolayer coating was then partially PEO-processed to achieve a $(\text{ZrO}_2, \text{Al}_2\text{O}_3) / (\text{Zr, Al})$ composite multilayer coating.

PEO treatments were carried out for 20 min in a homemade experimental set-up described in detail in a previous works [81, 82]. Before proceeding with PEO, all but the cold-sprayed face of the rectangular samples were masked using an epoxy resin to prevent them from oxidizing. The electrolytic solution consisted of potassium hydroxide KOH ($1 \text{ g.L}^{-1} \cong 0.018 \text{ mol.L}^{-1}$) and sodium silicate Na_2SiO_3 ($1.65 \text{ g.L}^{-1} \cong 0.014 \text{ mol.L}^{-1}$) diluted in deionized water. The resulting conductivity and pH were 7.5 mS.cm^{-1} and 12.5, respectively. Temperature of the electrolyte was maintained at $30 \text{ }^\circ\text{C}$. As presented in references [81, 82], the electrodes were supplied with a pulsed bipolar current. The anodic to cathodic charge quantity ratio, the anodic current density and the pulse frequency were set at 0.9, 65 A.dm^{-2} and 100 Hz, respectively. After PEO, the samples were rinsed with ethanol and dried under a warm air stream.

Samples produced after duplex cold-spray and PEO treatments were examined using a scanning electron microscope (FEG-SEM Philips XL 30S). Observations were performed in backscattered electrons imaging conditions (25 kV accelerating voltage) on the samples cross-section and in secondary electrons imaging conditions (5 kV) on the samples top surface. For the cross-section observations, the samples were previously hot mounted in resin and finely polished to achieve a mirror-like surface aspect. Prior to SEM examination samples were coated with a 10 nm carbon layer to avoid charging issues. Energy dispersive X-ray (EDX) analyses were conducted to estimate the chemical composition of the processed surfaces. In addition, EDX elemental mappings were carried out in order to image the spatial distribution

of elements throughout the coating thickness. X-ray diffraction (XRD) measurements (Bruker D8 ADVANCE diffractometer, Cu-K $_{\alpha 1}$ at 0.1541 nm) were performed to characterize the phase composition through the cold-sprayed coatings as well as through the PEO oxide layers. The scanning speed was set at 0.005° per second for a scan range 2 θ from 25 to 70°.

3. Results and discussion

3.1 Characterization of the cold-sprayed coatings

Figure 2 shows the visual aspect of the two series of samples. Just after performing the cold-spray deposition (fig. 2a and fig. 2c), the visual aspect of the samples appears homogeneous, suggesting a homogeneous covering of their surface with the metallic sprayed coating. The Zr sprayed coating appears dark-gray (fig. 2a) while the (Zr, Al) composite sprayed coating appears lighter (fig. 2c), as a result of the mixture between the dark-gray Zr sprayed particles and the silvery-coloured Al sprayed particles.

Figure 3 presents the results concerning the microstructural characterization of the Zr / Al metallic multilayer sprayed coating. The cross-sectional SEM micrograph (fig. 3a) evidences the high surface roughness of the steel substrate that was prepared by high-pressure cryogenic nitrogen jet prior to cold-spray deposition. On this prepared surface, a ~ 70 μm thick Al layer and a ~ 90 μm thick Zr layer were successively cold-spray deposited as shown in fig. 3a. The inner Al sublayer appears more compact than the outer Zr one. This can be explained by considering the mechanical properties of the sprayed powders [83, 84]. Indeed, the lower hardness and the lower yield stress of the Al sprayed particles (~ 50 Hv and ~ 130 MPa, respectively), compared to the Zr particles (~ 170 Hv and ~ 230 MPa, respectively), promote their plastic deformation during impact, and thus their adhesion on the substrate to form a denser coating. By contrast, a significant amount of the Zr particles rebound off the surface

and their limited plastic deformation not only affects the deposition efficiency, but it also results in an extended level of porosity through the sprayed coating associated with a higher surface roughness. This porosity is also clearly observable from the top surface SEM micrograph given in fig. 3e. EDX spectra recorded on the substrate (spot 1 in fig. 3a), the inner (spot 2) and the outer (spot 3) sublayers, are displayed in fig. 3c and fig. 3f. They show that spots 1, 2 and 3 are composed of iron, aluminium and zirconium, respectively. This is particularly obvious in fig. 3d that shows the EDX elemental mappings in Fe, Al, Zr and O elements (the probed area is indicated by the yellow dashed rectangle in fig. 3a). It is worth noting that oxygen is also detected in a significant proportion throughout the zirconium outer sublayer. This is explained by considering the highly porous morphology of the zirconium outer sublayer that allows the thermoplastic mounting resin to deeply penetrate pores during the hot mounting procedure of the sample. Besides these chemical analyses, the XRD pattern recorded on the Zr / Al metallic multilayer sprayed coating (fig. 3b) confirms the presence of zirconium in the outer sublayer but also shows the presence of zirconium hydrides (ZrH and ZrH₂). Zirconium and hydrogen having a strong affinity at room temperature, the presence of zirconium hydrides in the sprayed zirconium coating can be explained by the partial hydrogenation of the zirconium metallic powder during its storage in air and at ambient conditions [85, 86]. The presence of zirconium hydrides into the Zr-sprayed particles may explain the brown-coloured visual aspect of the Zr sprayed coating observed in fig. 2a.

Figure 4 gathers the results related to the microstructural characterization of the (Zr, Al) metallic monolayer sprayed coating. This coating has a thickness of about 100 μm . This cold-sprayed layer, mixing Zr and Al, appears more compact than the Zr outer sublayer observed in fig. 3a. This observation can be explained by considering differences in the density and in the mechanical properties between the Al and Zr metallic co-sprayed particles. The addition of denser and harder Zr particles ($\sim 6.5 \text{ g/cm}^3$ and $\sim 170 \text{ Hv}$, respectively) into the lighter-weight

and softer Al powder ($\sim 2.7 \text{ g/cm}^3$ and $\sim 50 \text{ Hv}$, respectively) helps improving the coating deposition as well as decreasing the coating porosity owing to a densification mechanism. This is likely due to the larger peening effect of the Zr particles caused by their higher kinetic energy combined with their higher hardness [87-89]. Figure 4 shows that the coating consists of irregularly shaped and fragmented particles with an average diameter of about $30 \mu\text{m}$ that are embedded in a darker matrix. This morphological aspect is also observable from the top surface SEM micrograph given in fig. 4e. The EDX spectra (fig. 4c and fig. 4f) show that the fragmented particles (spot 6 in fig. 4a) and the surrounding matrix (spot 5 in fig. 4a) are composed of zirconium and aluminium, respectively. Although the volume proportion of the sprayed zirconium powder was set at 50 %, image processing performed on cross-sectional SEM micrographs evidences that the volume proportion of zirconium particles really incorporated in the produced coating is about 38 %. This is due to the lower ductility of zirconium (as well as the zirconium hydrides contained in the zirconium particles) compared to aluminium, which results in a lower deposition rate [83, 84, 90, 91].

3.2 Characterization of the PEO oxidized coatings

Figure 2(b, d) show the visual aspects of the cold-sprayed samples after PEO treatment. From a general point of view, the dark initial aspect of the as-sprayed coatings due to zirconium sprayed particles (fig. 2(a,c)) turns into a lighter aspect. This is a visual characteristic of the presence of ceramic oxides over the processed surface, zirconium oxide and aluminium oxide having both a white matte color. This first observation suggests that oxidation took place during the PEO treatment. This is particularly obvious in the case of the Zr/Al sprayed coating for which the typical dark-gray aspect of the cold-sprayed zirconium (fig. 2a) turns into the light gray-coloured aspect of zirconium oxide (fig. 2b). Additionally, after PEO, the visual aspect of the samples remains quite homogeneous over the surface also suggesting a quite homogeneous PEO processing of the surface. Particularly, the present PEO

processed samples do not exhibit an inhomogeneous PEO treatment between the edges and the centre of samples as usually encountered with PEO process [92]. This is explained by the fact that before PEO, edges of the samples were protected with an epoxy resin, thus avoiding this edge effect during the PEO process.

Figure 5 displays the results of the microstructural characterization of the Zr / Al metallic multilayer sprayed coating after PEO treatment. The cross-sectional (fig. 5a) and top surface (fig. 5e) SEM micrographs show that the outer Zr cold-sprayed layer was partially converted into an oxide outer sublayer, giving rise to a ceramic/metal composite multilayer on steel. About 60 μm of the outer Zr layer was converted, thus leaving an intermediate Zr sublayer of about 30 μm in thickness. Figure 5a also shows the presence of unconverted particles remaining throughout the oxide outer sublayer. This can be explained by the fact that during the PEO treatment, large size Zr particles or aggregated Zr particles had not enough time to completely be converted into an oxide, since oxidation takes place first at the shell of the particles, thus leaving the core unconverted. Such an explanation is in good agreement with other published works on the oxidation behaviour of (Ti, Al)-based composite coatings prepared by cold spray [93-95]. Additionally, cracks appear in the Al cold-sprayed inner sublayer because of the development of strong internal compressive stresses during the formation of the oxide outer sublayer. The high proportion of the monoclinic form of zirconium oxide m-ZrO₂ (fig. 5b) evidences that the cold-sprayed Zr layer was partially converted into monoclinic zirconium oxide during the PEO process. It is worth mentioning that, although only m-ZrO₂ was identified from XRD measurements, the presence of the metastable tetragonal form t-ZrO₂ in a very small amount may not be excluded as discussed in reference [44]. Low intensity XRD peaks of zirconium and zirconium hydrides are also observed, which confirms the presence in lower proportion of unconverted zirconium cold-sprayed particles in the outer oxide sublayer. The EDX spectra (fig. 5c) and the EDX

elemental mappings for Fe, Al, Zr, O (fig. 5d) confirm the presence of a zirconium oxide layer on the zirconium layer. Particularly, the EDX spectrum recorded on the outer sublayer (spot 10 in fig. 5c) evidences the presence of Zr and O while the spectrum recorded on the intermediate sublayer (spot 9 in fig. 5c) shows the exclusive presence of Zr. Moreover, and as usually encountered for PEO coatings prepared in silicate electrolyte, the EDX spectrum recorded on the topmost surface and displayed in fig. 5f shows that Si element incorporates through the thin outermost zirconia layer in contact with the electrolyte [46, 50, 57]. Finally, all these microstructural characterizations of the PEO-processed Zr / Al metallic multilayer cold-sprayed coating evidence the feasibility of elaborating a ZrO_2 / Zr / Al composite multilayer coating on steel.

The results from the microstructural characterization of the (Zr, Al) metallic monolayer cold-sprayed coating after PEO treatment are gathered in fig. 6. The cross-sectional (fig. 6a) and top surface (fig. 6e) SEM micrographs show that the (Zr, Al) monolayer was partially converted into an oxide layer of about 30 μm in thickness, thus leaving an intermediate (Zr, Al) sublayer of about 70 μm thick. This outer PEO coating consists of light and dark diffuse areas that penetrate each other suggesting an interpenetration of aluminium oxide (dark areas) with zirconium oxide (light areas). This is in contrast to the (Zr, Al) metallic inner sublayer where Zr and Al cold-sprayed particles appear well delimited. Additionally and as previously observed in fig. 5a, the SEM micrograph also shows that some Zr particles are not fully converted into oxide throughout the outer PEO sublayer. These untreated particles are found in the diffuse light areas in fig. 6a. It is also noticeable that no crack is observed in the initial cold-sprayed coating, and no delamination is detected as well between the steel substrate and the overall multilayer coating. The XRD pattern recorded on the produced duplex coating is displayed in fig. 6b. Besides the presence of zirconium and zirconium hydrides (ZrH and ZrH_2) related to unconverted particles, the XRD pattern shows the formation of both

zirconium oxide (monoclinic $m\text{-ZrO}_2$) and aluminium oxides (the face-centred cubic $\eta\text{-Al}_2\text{O}_3$ and the rhombohedral corundum $\alpha\text{-Al}_2\text{O}_3$) in the outer PEO sublayer. The EDX spectra and the EDX elemental mappings of Fe, Al, Zr and O given in fig. 6c and fig. 6d, respectively, complete these observations. Particularly, the EDX spectrum recorded in a diffuse lightened area (spot 14 in fig. 6c) shows that it mainly consists of Zr and O as well as Al, to a lesser extent. Combined with previous XRD measurements, it suggests that these diffuse lightened areas are composed of a high phase proportion of zirconium oxide mixed with a low phase proportion of aluminium oxide. Inversely, in a diffuse darkened area (spot 15 in fig. 6c), the EDX spectrum shows that it mainly consists of Al and O as well as Zr, to a lesser extent. It suggests that these diffuse darkened areas are composed of a high phase proportion of aluminium oxide mixed with a low phase proportion of zirconium oxide. EDX spectra recorded from the top surface on these two different area also show that Si, K and Na elements initially dissolved into the electrolyte are found in the outermost layer (fig. 6f). Peak intensity of these elements appear higher in the alumina enriched areas than in the zirconia ones suggesting thereby a higher incorporation in the “pancake” like structure of the alumina enriched areas. Finally, all the microstructural characterizations carried out on the PEO processed (Zr, Al) metallic monolayer cold-sprayed coating evidence the feasibility of elaborating a $(\text{ZrO}_2, \text{Al}_2\text{O}_3) / (\text{Zr}, \text{Al})$ composite multilayer coating on steel.

4. Conclusion

The feasibility of elaborating $(\text{ZrO}_2, \text{Al}_2\text{O}_3) / (\text{Zr}, \text{Al})$ composite multilayer coatings on steel by combining cold-spray deposition and plasma electrolytic oxidation (PEO) methods was investigated. For this purpose, before performing PEO, zirconium and aluminium powders were cold-sprayed on steel into two different configurations. The first configuration consisted in subsequently cold-spraying a Zr / Al metallic multilayer coating while the second

consisted in simultaneously cold-spraying a (Zr, Al) metallic monolayer coating. For the first configuration, after duplex cold-spray and PEO processing, results clearly demonstrate the possibility of elaborating a $ZrO_2 / Zr / Al$ composite multilayer coating on steel. For the second configuration, results also evidence the possibility of elaborating a $(ZrO_2, Al_2O_3) / (Zr, Al)$ composite multilayer coating on steel. Such a duplex treatment combining cold-spray and PEO offers new opportunities to protect the surface of non-valve metals for which direct PEO process is unsuitable, as well as to emerge new functional properties. At this point, further investigations must be carried out to study the properties of such duplex coatings such as wear resistance and corrosion resistance.

Acknowledgments

- This work was supported by the French Government through the programme "Investissements d'avenir" operated by the French National Research Agency (ANR) and referenced to as ANR-11-LABX-0008-01 ('LabEx DAMAS').
- This work was also partly supported by the Conseil Régional de la Région Grand Est granted C. Da Silva Tousch PhD work under decision 19_GE8_049.
- This work was also partly supported by the Institut Carnot ICEEL within the "SOPRODSYSE" and "MATITHY" projects.
- The authors would like to acknowledge contributions of the following:
 - The competence cluster on X-ray diffraction (CC-X γ) at Institut Jean Lamour for providing advices in XRD measurements and analyses.
 - The competence cluster on electron microscopy (CC 3M) at Institut Jean Lamour for providing advices in SEM observations and EDX analyses.
 - The research centre CRITT TJFU for preparing substrate surfaces by using nitrogen jets under supercritical pressures and for preparing cold-sprayed coatings.

Data availability

The data that support the findings of this study are available from the corresponding author upon reasonable request.

Contribution of each author

J. Martin, T. Czerwiec and G. Henrion conceptualized the goal of this research work.

G. Henrion and J. Martin conceived the PEO experimental rigs.

J. Martin and A. Maizeray ensured the production of the cold-sprayed coatings in collaboration with CRITT TJFU.

J. Martin, A. Maizeray and C. Da Silva Tousch performed the PEO experiments.

J. Martin, A. Maizeray and C. Da Silva Tousch performed the material characterizations.

J. Martin prepared the manuscript.

All the authors analysed the results and reviewed the manuscript.

J. Martin, G. Marcos, T. Czerwiec and G. Henrion supervised the whole work.

Additional information

The authors declare no competing financial interests.

List of references

- [1] D. Dwivedi, K. Lepková, T. Becker, Carbon steel corrosion: a review of key surface properties and characterization methods, *RSC Adv.* 7 (2017) 4580-4610.
- [2] M.H. Shahini, H. Eivaz Mohammadloo, B. Ramezanzadeh, Recent advances in steel surface treatment via novel/green conversion coatings for anti-corrosion applications: a review study, *J. Coat. Technol. Res.* 19 (2022) 159-199.
- [3] C.J. Scheuer, R.P. Cardoso, S.F. Brunatto, An overview on plasma assisted thermochemical treatments of martensitic stainless steels, *Surf. Topogr.- Metrol. Prop.* 11 (2023) 013001.
- [4] D. Wang, G.P. Bierwagen, Sol-gel coatings on metals for corrosion protection, *Prog. Org. Coat.* 64 (2009) 327-338.
- [5] A. Mavrič, M. Valant, C. Cui, Z.M. Wang, Advanced applications of amorphous alumina: from nano to bulk, *J. Non Cryst. Solids* 521 (2019) 119493.
- [6] P.P. Dey, S. Sahu, P.S. Banerjee, M. Ghosh, A review on metallurgical features of hot-dip aluminized steel, *Eng. Res. Express* 5 (2023) 012002.
- [7] J. Meyer, P. Görn, F. bertram, S. Hamwi, T. Winkler, H.H. Johannes, T. Weimann, T. Riedl, W. Kowalsky, Al₂O₃/ZrO₂ nanolaminates as ultrahigh gas-diffusion barriers – A strategy for reliable encapsulation of organic electronics, *Adv. Mater.* 21 (2009) 1845-1849.
- [8] S. Lee, H. Choi, S. Shin, J. Park, G. Ham, H. Jung, H. Jeon, Permeation barrier properties of an Al₂O₃/ZrO₂ multilayer deposited by remote plasma atomic layer deposition, *Curr. Appl. Phys.* 14 (2014) 552-557.
- [9] R. Yin, L. Hu, J. Tang, T. Cheng, D. Zhang, G. Zhang, Z. Chen, M. Hong, G. Cai, Y. Shi, C. Jiang, F. Ren, In-situ oxidation of aluminized stainless-steel to form alumina as tritium permeation barrier coating, *Fusion Eng. Des.* 163 (2021) 112154.

- [10] X. Lu, M. Mohedano, C. Blawert, E. Matykina, R. Arrabal, K. U. Kainer, M. L. Zheludkevich, Plasma electrolytic oxidation coatings with particle additions – A review, *Surf. Coat. Technol.* 307 (2016) 1165-1182.
- [11] M. Kaseem, Y.H. Lee, Y.G. Ko, Incorporation of MoO₂ and ZrO₂ particles into the oxide film formed on 7075 Al alloy via micro-arc oxidation, *Mater. Lett.* 182 (2016) 260-263.
- [12] M. Kaseem, M.O. Kamil, Y.G. Ko, Electrochemical response of MoO₂-Al₂O₃ oxide films via plasma electrolytic oxidation, *Surf. Coat. Technol.* 322 (2017) 163-173.
- [13] M. Kaseem, Y.G. Ko, Electrochemical response of Al₂O₃-MoO₂-TiO₂ oxide films formed on 6061 Al alloy by plasma electrolytic oxidation, *J. Electrochem. Soc.* 163 (2016) C587-C592.
- [14] M. Kaseem, T. Hussain, U.R. Zeeshan, H.W. yang, B. Dikici, Y.G. Ko, Fabrication of functionalized coating with a unique flowery-flake structure for an effective corrosion performance and catalytic degradation, *Chem. Eng. J.* 420 (2021) 129737.
- [15] M. Kaseem, S. Fatimah, N. Nashrah, Y.G. Ko, Recent progress in surface modification of metals coated by plasma electrolytic oxidation: principle, structure, and performance, *Prog. Mater. Sci* 117 (2021) 100735.
- [16] P.Y. Gao, Y.D. Ma, W.W. Sun, Y. Yang, C. Zhang, Y.H. Cui, Y.W. Wang, Y.C. Dong, Microstructure and properties of Al₂O₃-ZrO₂-TiO₂ composite coatings prepared by plasma spraying, *Rare Met.* 40 (2021) 1825–1834.
- [17] C. Exare, J.-M. Kiat, N. Guiblin, F. Porcher, V. Petricek, Structural evolution of ZTA composites during synthesis and processing, *J. Eur. Ceram. Soc.* 35 (2015) 1273-1283.

- [18] J. Kiilakoski, R. Musalek, F. Lukac, H. Koivuluoto, P. Vuoristo, Evaluating the toughness of APS and HVOF-sprayed $\text{Al}_2\text{O}_3\text{-ZrO}_2$ -coatings by in-situ- and macroscopic bending, *J. Eur. Ceram. Soc.* 38 (2018) 1908-1918.
- [19] Y. Yan, Y. Han, D. Li, J. Huang, Q. Lian, Effect of NaAlO_2 concentrations on microstructure and corrosion resistance of $\text{Al}_2\text{O}_3/\text{ZrO}_2$ coatings formed on zirconium by micro-arc oxidation, *Appl. Surf. Sci.* 256 (2010) 6359-6366.
- [20] S. Sathishi, M. Geetha, Comparative study on corrosion behavior of plasma sprayed Al_2O_3 , ZrO_2 , $\text{Al}_2\text{O}_3/\text{ZrO}_2$ and $\text{ZrO}_2/\text{Al}_2\text{O}_3$ coatings, *Trans. Nonferrous Met. Soc. China* 26 (2016) 1336-1344.
- [21] P. Wang, S. Deng, Y. He, C. Liu, J. Zhang, Oxidation and hot corrosion behavior of $\text{Al}_2\text{O}_3/\text{YSZ}$ coatings prepared by cathode plasma electrolytic deposition, *Corros. Sci.* 109 (2016) 13-21.
- [22] F. Kern, P. Palmero, F. Garcia Marro, A. Mestra, Processing of alumina-zirconia composites by surface modification route with enhanced hardness and wear resistance, *Ceram. Int.* 41 (2015) 889-898.
- [23] S. Mohamed Abbas, A. Elayaperumal, S. Arulvel, Enhancement of the hardness and wear-resistance of aluminum-silicon alloy using atmospheric plasma-sprayed ZrO_2 , $\text{Al}_2\text{O}_3\text{-ZrO}_2$ multilayer, and $\text{Al}_2\text{O}_3/\text{ZrO}_2$ composite coatings, *Surf. Topogr. - Metrol. Prop.* 8 (2020) 025027.
- [24] M. Nejati, M.R. Rahimipour, I. Mobasherpour, A.H. Pakseresht, Microstructural analysis and thermal shock behavior of plasma sprayed ceria-stabilized zirconia thermal barrier coatings with micro and nano Al_2O_3 as a third layer, *Surf. Coat. Technol.* 282 (2015) 129-138.

- [25] B. Gao, X. Sun, C. Yao, L. Mao, A new strategy to obtain thin $\text{ZrO}_2\text{-Al}_2\text{O}_3$ composite aerogel coating with prominent high-temperature resistance and rapid heat dissipation, *J. Solid State Chem.* 314 (2022) 123384.
- [26] J. Bartolomé, C. Pecharromán, J. Moya, A. Martín, J.Y. Pastor, J. Llorca, Percolative mechanism of sliding wear in alumina/zirconia composites, *J. Eur. Ceram. Soc.* 26 (2006) 2619-2625.
- [27] T. Douillard, J. Chevalier, A. Descamps-Mandine, I. Warber, Y. Galais, P. Whitaker, J.J. Wu, Q.Q. Wang, Comparative ageing behaviour of commercial unworn and worn 3Y-TZP and zirconia-toughened alumina hip joints heads, *J. Eur. Ceram. Soc.* 32 (2012) 1529-1540.
- [28] Y. Wang, M. Wang, Z. Jiang, Microstructure and corrosion resistance of $\text{Al}_2\text{O}_3\text{-ZrO}_2$ composite coating on biomedical magnesium alloy fabricated by cathodic plasma electrolytic oxidation, *Appl. Mech. Mater.* 184 (2012) 1068-1071.
- [29] L. Zhang, W. Zhang, Y. Han, W. Tang, A nanoplate-like $\alpha\text{-Al}_2\text{O}_3$ out-layered $\text{Al}_2\text{O}_3\text{-ZrO}_2$ coating fabricated by micro-arc oxidation for hip joint prosthesis, *Appl. Surf. Sci.* 361 (2016) 141-149.
- [30] P. Ramaswamy, S. Seetharamu, K.B.R. Varma, K.J. Rao, $\text{Al}_2\text{O}_3\text{-ZrO}_2$ composite coatings for thermal-barrier applications, *Compos. Sci. Technol.* 57 (1997) 81-89.
- [31] A. Keyvani, Microstructural stability oxidation and hot corrosion resistance of nanostructured $\text{Al}_2\text{O}_3\text{/YSZ}$ composite compared to conventional YSZ TBC coatings, *J. Alloy. Compd.* 623 (2015) 229-237.
- [32] A. Portinha, V. Teixeira, J. O. Carneiro, S. N. Dub, R. Shmegeera, C. J. Tavares, Hard $\text{ZrO}_2\text{/Al}_2\text{O}_3$ nanolaminated PVD coatings evaluated by nanoindentation, *Surf. Coat. Technol.* 200 (2005) 765-768.

- [33] N. Schalk, M. Tkadletz, C. Mitterer, Hard coatings for cutting applications: physical vs chemical vapor deposition and future challenges for the coatings community, *Surf. Coat. Technol.* 429 (2022) 127949.
- [34] S. J. Park, D. J. Choi, Synthesis of porous $\text{Al}_2\text{O}_3/\text{ZrO}_2$ nanocomposites by chemical vapour deposition, *Adv. Appl. Ceram.* 116 (2017) 263-241.
- [35] A.L. Vasiliev, N.P. Padture, X. Ma, Coatings of metastable ceramics deposited by solution-precursor plasma spray: I. Binary $\text{ZrO}_2\text{-Al}_2\text{O}_3$ system, *Acta Mater.* 54 (2006) 4913-4920.
- [36] N. Dejang, A. Limpichaipanit, A. Watcharapasorn, S. Wirojanupatump, P. Niranatlumpong, S. Jiansirisomboon, Fabrication and properties of plasma-sprayed $\text{Al}_2\text{O}_3/\text{ZrO}_2$ composite coatings, *J. Therm. Spray Technol.* 20 (2011) 1259-1268.
- [37] J.S Hong, S.D. Torre, L. Gao, K. Miyamoto, H. Miyamoto, Synthesis and mechanical properties of $\text{ZrO}_2/\text{Al}_2\text{O}_3$ composites prepared by spark plasma sintering, *J. Mater. Sci. Lett.* 17 (1998) 1313-1315.
- [38] Y.X. Hao, J.S. Li, X.J. Yang, X. Wang, L.D. Lu, Preparation of $\text{ZrO}_2\text{-Al}_2\text{O}_3$ composite membranes by sol-gel process and their characterization, *Mater. Sci. Eng. A - Struct. Mater. Prop. Microstruct. Process.* 367 (2004) 243-247.
- [39] B.T. Lee, J.K. Han, F. Saito, Microstructure of sol-gel synthesized $\text{Al}_2\text{O}_3\text{-ZrO}_2(\text{Y}_2\text{O}_3)$ nano-composites studied by transmission electron microscopy, *Mater. Lett.* 59 (2005) 355-360.
- [40] B. Liang, G. Zhang, H.L. Liao, C. Coddet, C.X. Ding, Friction and wear behavior of $\text{ZrO}_2\text{-Al}_2\text{O}_3$ composite coatings deposited by air plasma spraying: Correlation with physical and mechanical properties, *Surf. Coat. Technol.* 203 (2009) 3253-3242.

- [41] Y.Y. Yan, Y. Han, J.J. Huang, Formation of Al₂O₃-ZrO₂ composite coating on zirconium by micro-arc oxidation, *Scr. Mater.* 59 (2008) 203-206.
- [42] Gh. Barati Darband, M. Aliofkhaezai, P. Hamghalam, N. Valizade, Plasma electrolytic oxidation of magnesium and its alloys: Mechanism, properties and applications, *J. Magnes. Alloy.* 5 (2017) 74-132.
- [43] Y. L. Cheng, J. Cao, M. Mao, H. Xie, P. Skeldon, Key factors determining the development of two morphologies of plasma electrolytic coatings on an Al-Cu-Li alloy in aluminate electrolytes. *Surf. Coat. Technol.* 291 (2016) 239-249.
- [44] Y. L. Cheng, J. Cao, Z. Peng, Q. Wang, E. Matykina, P. Skeldon, G. E. Thompson. Wear resistant coatings formed on Zircaloy-2 by plasma electrolytic oxidation in sodium aluminate electrolytes. *Electrochim. Acta* 116 (2014) 453-466.
- [45] A. Mathis, E. Rocca, D. Veys-Renaux, J. Tardelli, Electrochemical behaviour of titanium in KOH at high potential, *Electrochim. Acta* 202 (2016) 253-261.
- [46] A. L. Yerokhin, X. Nie, A. Leyland, A. Matthews, S. J. Dowey, Plasma electrolysis for surface engineering, *Surf. Coat. Technol.* 122 (1999) 73-93.
- [47] M. Molaei, K. Babaei, A. Fattah-alhosseini, Improving the wear resistance of plasma electrolytic oxidation (PEO) coating applied on Mg and its alloys under the addition of nano- and micro-sized additives into the electrolytes: A review, *J. Magnes. Alloy.* 9 (2021) 1164-1186.
- [48] A. Buling, J. Zerrer, Increasing the application fields of magnesium by ultracermic[®]: Corrosion and wear protection by plasma electrolytical oxidation (PEO) of Mg alloys, *Surf. Coat. Technol.* 369 (2019) 142-155.

- [49] K. Ling, Q. Mo, X. Lv, G. Qin, W. Yang, L. Li, W. Li, Growth characteristics and corrosion resistance of micro-arc oxidation coating on Al-Mg composite plate, *Vacuum* 195 (2022) 110640.
- [50] J. A. Curran, H. Kalkanci, Y. Magurova, T. W. Clyne, Mullite-rich plasma electrolytic oxide coatings for thermal barrier applications, *Surf. Coat. Technol.* 201 (2007) 8683-8687.
- [51] Q. Xia, D. Zhang, D. Li, Z. Jiang, Z. Yao, Preparation of the plasma electrolytic oxidation coating on Mg-Li alloy and its thermal control performance, *Surf. Coat. Technol.* 369 (2019) 252-256.
- [52] F. Muhaffel, M. Bayogan, H. Cimenoglu, A study to enhance the mechanical durability of the MAO coating fabricated on the 7075 Al alloy for wear-related high temperature applications, *Surf. Coat. Technol.* 409 (2021) 126843.
- [53] L. Pezzato, K. Brunelli, S. Diodati, M. Pigato, M. Bonesso, M. Dabalà, Microstructural and corrosion properties of hydroxyapatite containing PEO coating produced on AZ31 Mg alloy, *Materials* 14 (2021) 1531-1545.
- [54] L. V. Parfenova, E. S. Lukina, Z. R. Galimshina, G. U. Gil'fanova, V. R. Mukaeva, R.G. Farrakhov, K.V. Danilko, G.S. Dyakonov, E.V. Parfenov, Biocompatible organic coatings based on bisphosphonic acid RGD-derivatives for PEO-modified titanium implants, *Molecules* 25 (2020) 229-250.
- [55] M. Coto, S. C. Troughton, P. Knight, R. Joshi, R. Francis, R. V. Kumar, T. W. Clyne, Optimization of the microstructure of TiO₂ photocatalytic surfaces created by Plasma Electrolytic Oxidation of titanium substrates, *Surf. Coat. Technol.* 411 (2021) 127000.
- [56] S. Stojadinović, N. Radić, N. Tadić R. Vasilić, B. Grbić, Enhanced ultraviolet light driven photocatalytic activity of ZnO particles incorporated by plasma electrolytic oxidation into Al₂O₃ coatings co-doped with Ce³⁺, *Opt. Mater.* 101 (2020) 109768.

- [57] J. Martin, A. Nominé, V. Ntomprougkidis, S. Migot, S. Bruyère, F. Soldera, T. Belmonte, G. Henrion, Formation of a metastable nanostructured mullite during Plasma Electrolytic Oxidation of aluminium in “soft” regime condition, *Mater. Design* 180 (2019) 107977.
- [58] A. L. Yerokhin, L. O. Snizhko, N. L. Gurevina, A. Leyland, A. Pilkington, A. Matthews, Discharge characterization in plasma electrolytic oxidation of aluminium, *J. Phys. D: Appl. Phys.* 36 (2003) 2110–2120.
- [59] R. O. Hussein, X. Nie, D. O. Northwood, A. Yerokhin, A. Matthews, Spectroscopic study of electrolytic plasma and discharging behaviour during the plasma electrolytic oxidation (PEO) process, *J. Phys. D: Appl. Phys.* 43 (2010) 105203.
- [60] J. Jovović, S. Stojadinović, N. M. Šišović, N. Konjević, Spectroscopic study of plasma during electrolytic oxidation of magnesium- and aluminium-alloy, *J. Quant. Spectrosc. Rad. Trans.* 113 (2012) 1928-1937.
- [61] S. Stojadinović, J. Jovović, M. Petković, R. Vasilić, N. Konjević, Investigation of plasma electrolytic oxidation on valve metals by means of molecular spectroscopy – a review, *RSC Adv.* 4 (2014) 25759-25789.
- [62] T. W. Clyne, S. C. Troughton, A review of recent work on discharge characteristics during plasma electrolytic oxidation of various metals, *Int. Mater. Rev.* 64 (2019) 127-162.
- [63] E. Matykina, R. Arrabal, P. Skeldon, G.E. Thompson, Incorporation of zirconia nanoparticles into coatings formed on aluminium by AC plasma electrolytic oxidation, *J. Appl. Electrochem.* 38 (2008) 1375-1383.
- [64] S. Fatimah, M.P. Kamil, J.H. Kwon, M. Kaseem, Y.G. Ko, Dual incorporation of SiO₂ and ZrO₂ nanoparticles into the oxide layer on 6061 Al alloy via plasma electrolytic oxidation : Coating structure and corrosion properties, *J. Alloy. Compd.* 707 (2017) 358-364.

- [65] N. Barati, E.I. Meletis, Al₂O₃-ZrO₂ nanocomposites coating on aluminium alloy by plasma electrolytic-electrophoretic hybrid process, *Mater. Today Commun.* 19 (2019) 1-11.
- [66] R. Askarnia, M. Sobhani, M. Zare, H. Aghamohammadi, H. Staji, incorporation of Al₂O₃ and ZrO₂ ceramics to AZ31 magnesium alloys composite coating using micro-arc oxidation method, *J. Mech. Behav. Biomed. Mater.* 141 (2023) 105784.
- [67] H. Luo, Q. Cai, J. He, B. Wei, Preparation and properties of composite ceramic coating containing Al₂O₃-ZrO₂-Y₂O₃ on AZ91D magnesium alloy by plasma electrolytic oxidation, *Curr. Appl. Phys.* 9 (2009) 1341-1346.
- [68] M. Tang, W. Li, H. Liu, L. Zhu, Preparation Al₂O₃/ZrO₂ composite coating in an alkaline phosphate electrolyte containing K₂ZrF₆ on aluminium alloy by microarc oxidation, *Appl. Surf. Sci.* 258 (2012) 5869-5875.
- [69] V. Shoaie-Rad, M.R. Bayati, H.R. Zargar, J. Javadpour, F. Golestani-Fard, In situ growth of ZrO₂-Al₂O₃ nano-crystalline ceramic coatings via micro arc oxidation of aluminum substrates, *Mater. Res. Bull.* 47 (2012) 1494-1499.
- [70] N. Barati, E.I. Meletis, F. Golestani Fard, A. Yerokhin, S. Rastegari, M.A. Faghihi-Sani, Al₂O₃-ZrO₂ nanostructured coatings using DC plasma electrolytic oxidation to improve tribological properties of Al substrates, *Appl. Surf. Sci.* 356 (2015) 927-934.
- [71] N. Barati, A. Yerokhin, F. Golestanifard, S. Rastegari, E.I. Meletis, Alumina-zirconia coatings produced by Plasma Electrolytic Oxidation on Al alloy for corrosion resistance improvement, *J. Alloy. Compd.* 724 (2017) 435-442.
- [72] V. Malinovschi, A. Marin, D. Negrea, V. Andrei, E. Coaca, C.N. Milhailescu, C.P. Lungu, Characterization of Al₂O₃/ZrO₂ composite coatings deposited on Zr-2.5Nb alloy by plasma electrolytic oxidation, *Appl. Surf. Sci.* 451 (2018) 169-179.

- [73] S. Gowtham, S. Hariprasad, T. Arunnellaiappan, N. Rameshbabu, An investigation on ZrO₂ nano-particle incorporation, surface properties and electrochemical corrosion behaviour of PEO coating formed on Cp-Ti, *Surf. Coat. Technol.* 313 (2017) 263-273.
- [74] M. O'Hara, S.C. Troughton, R. Francis, T.W. Clyne, The incorporation of particles suspended in the electrolyte into plasma electrolytic oxidation coatings in Ti and Al substrates, *Surf. Coat. Technol.* 385 (2020) 125354.
- [75] X.M. Zhang, D.F. Chen, C.Z. Gong, S.Q. Yang, X.B. Tian, Modulation effects of K₂ZrF₆ additive on microstructure and heat resistance of micro-arc oxide coatings fabricated on LY12 aluminium alloy, *J. Inorg. Mater.* 25 (2010) 865-870.
- [76] Z. Ur Rehman, S.H. Shin, M. Kaseem, M. Uzair, B.H. Koo, Towards a compact coating formed on Al6061 alloy in phosphate based electrolyte via two-step PEO process and K₂ZrF₆ additives, *Surf. Coat. Technol.* 328 (2017) 355-360.
- [77] S.G. Xin, R.G. Zhao, H. Du, L.X. Song, Prepare and formation mechanism of the zirconia coating on aluminium alloy by plasma electrolytic oxidation, *J. Inorg. Mater.* 24 (2009) 107-110.
- [78] P. Gupta, G. Tenhundfeld, E. O. Daigle, D. Ryabkov, Electrolytic plasma technology: Science and engineering - An overview, *Surf. Coat. Technol.* 201 (2007) 8746-8760.
- [79] J. Martin, K. Akoda, V. Ntomprougkidis, O. Ferry, A. Maizeray, A. Bastien, P. Brenot, G. Ezo'o, G. Henrion, Duplex surface treatment of metallic alloys combining cold-spray and plasma electrolytic oxidation technology, *Surf. Coat. Technol.* 392 (2020) 125756.
- [80] A. Tazibt, G. Ezo'o, Y. Khalsi, M. Yahiaoui, Dry surface preparation using supercritical cryogenic nitrogen jet improves the adhesion strength of cold gas sprayed coatings (SCNCS), *Mater. Sci. Forum* 941 (2018) 1668-1673.

- [81] J. Martin, A. Melhem, I. Shchedrina, T. Duchanoy, A. Nominé, G. Henrion, T. Czerwicz, T. Belmonte, Effects of electrical parameters on plasma electrolytic oxidation of aluminium, *Surf. Coat. Technol.* 221 (2013) 70-76.
- [82] V. Ntomprougkidis, J. Martin, A. Nominé, G. Henrion, Sequential run of the PEO process with various pulsed bipolar current waveforms, *Surf. Coat. Technol.* 374 (2019) 713-724.
- [83] F. Gärtner, T. Stoltenhoff, T. Schmidt, H. Kreye, The cold spray process and its potential for industrial applications, *J. Therm. Spray Technol.* 15 (2006) 223-232.
- [84] V. Champagne, D. Helfrich, The unique abilities of cold spray deposition, *Int. Mater. Rev.* 61 (2016) 437-455.
- [85] C. E. Ells, Hydride precipitates in zirconium alloys (A review), *J. Nucl. Mater.* 28 (1968) 129-151.
- [86] J. Bair, M. A. Zaeem, M. Tonks, A review on hydride precipitation in zirconium alloys, *J. Nucl. Mater.* 466 (2015) 12-20.
- [87] E. Irissou, J.-G. Legoux, B. Arsemault, C. Moreau, investigation of Al-Al₂O₃ cold spray coating formation and properties, *J. Thermal Spray Technol.* 16 (2007) 661-668.
- [88] K. Spencer, D.M. Fabijanic, M.-X. Zhang, The use of Al-Al₂O₃ cold spray coatings to improve the surface properties of magnesium alloys, *Surf. Coat. Technol.* 204 (2009) 336-344.
- [89] Q. Wang, K. Spencer, N. Birbilis, M.-X. Zhang, The influence of ceramic particles on bond strength of cold spray composite coatings on AZ91 alloy substrate, *Surf. Coat. Technol.* 205 (2010) 50-56.
- [90] A. Moridi, S. M. Hassani-Gangaraj, M. Guagliano, M. Dao, Cold spray coating: review of material systems and future perspectives, *Surf. Eng.* 30 (2014) 369-395

- [91] M. Jeandin, G. Rolland, L. L. Descurninges, M. H. Berger, Which powders for cold spray?, *Surf. Eng.* 30 (2014) 291-298.
- [92] A. Melhem, G. Henrion, T. Czerwicz, J.L. Briançon, T. Duchanoy, F. Brochard, T. Belmonte, Changes induced by process parameters in oxide layers grown by the PEO process on Al alloys, *Surf. Coat. Technol.* 205 (2011) S133-S136.
- [93] T. Novoselova, S. Celotto, R. Morgan, P. Fox, W. O'Neill, Formation of TiAl intermetallics by heat treatment of cold-sprayed precursor deposits, *J. Alloy. Compd.* 436 (2007) 69-77.
- [94] L.Y. Kong, L. Shen, B. Lu, R. Yang, X.Y. Cui, T.F. Li, T.Y. Xiong, Preparation of TiAl₃-Al composite coating by cold spray and its high temperature oxidation behavior, *J. Therm. Spray Technol.* 19 (2010) 1206-1210.
- [95] H.Y. Lee, S.H. Jung, S.Y. Lee, K.H. Ko, Fabrication of cold-sprayed Al-intermetallic compounds coatings by post annealing, *Mater. Sci. Eng. A* 433 (2006) 139-143.

List of tables

Table 1: Elemental composition of the commercial S235 steel substrate

Elements	Mn	C	Si	P	S	Fe
in wt.%	1.4	0.17	0.05	0.035	0.035	Balance

Table 2: Elemental composition of the commercial 1050 aluminium cold-sprayed powder.

Elements	Fe	Si	Zn	Cu, Mg, Mn, Ti	Al
in wt.%	0.40	0.25	0.07	<0.05	Balance

Table 3: Elemental composition of the commercially pure zirconium cold-sprayed powder.

Elements	O	Fe	Cr	Zr
in wt.%	0.035	0.012	<0.01	Balance

List of figures

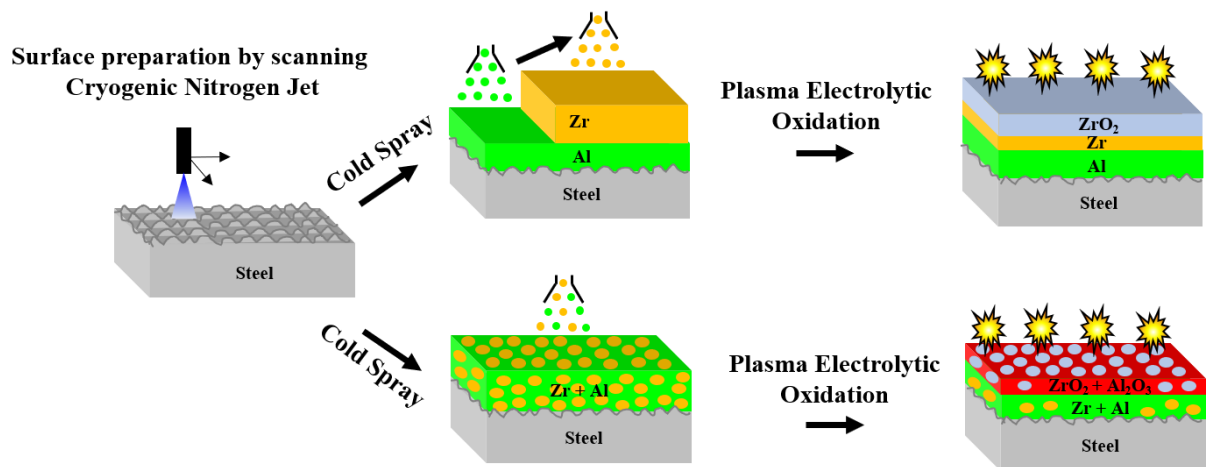


Figure 1: Schematic description of the duplex surface treatments carried out on steel (prepared with cryogenic nitrogen jet) combining cold spray and plasma electrolytic oxidation, in the case of a cold-sprayed Zr / Al metallic multilayer coating, and a cold-sprayed (Zr, Al) metallic composite monolayer coating.

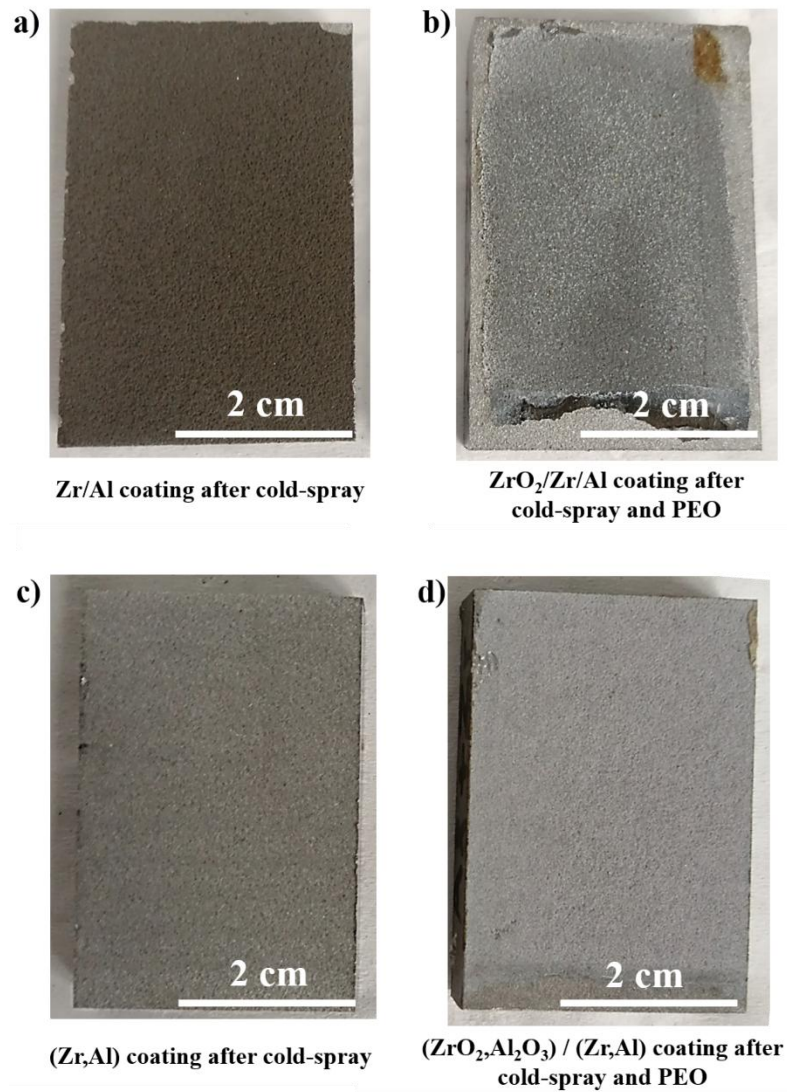


Figure 2: Visual aspect of the samples produced by cold-spraying a Zr / Al metallic multilayer coating on a steel substrate **a)** before and **b)** after plasma electrolytic oxidation (PEO), and by cold-spraying a (Zr, Al) metallic composite monolayer coating on a steel substrate **c)** before and **d)** after PEO.

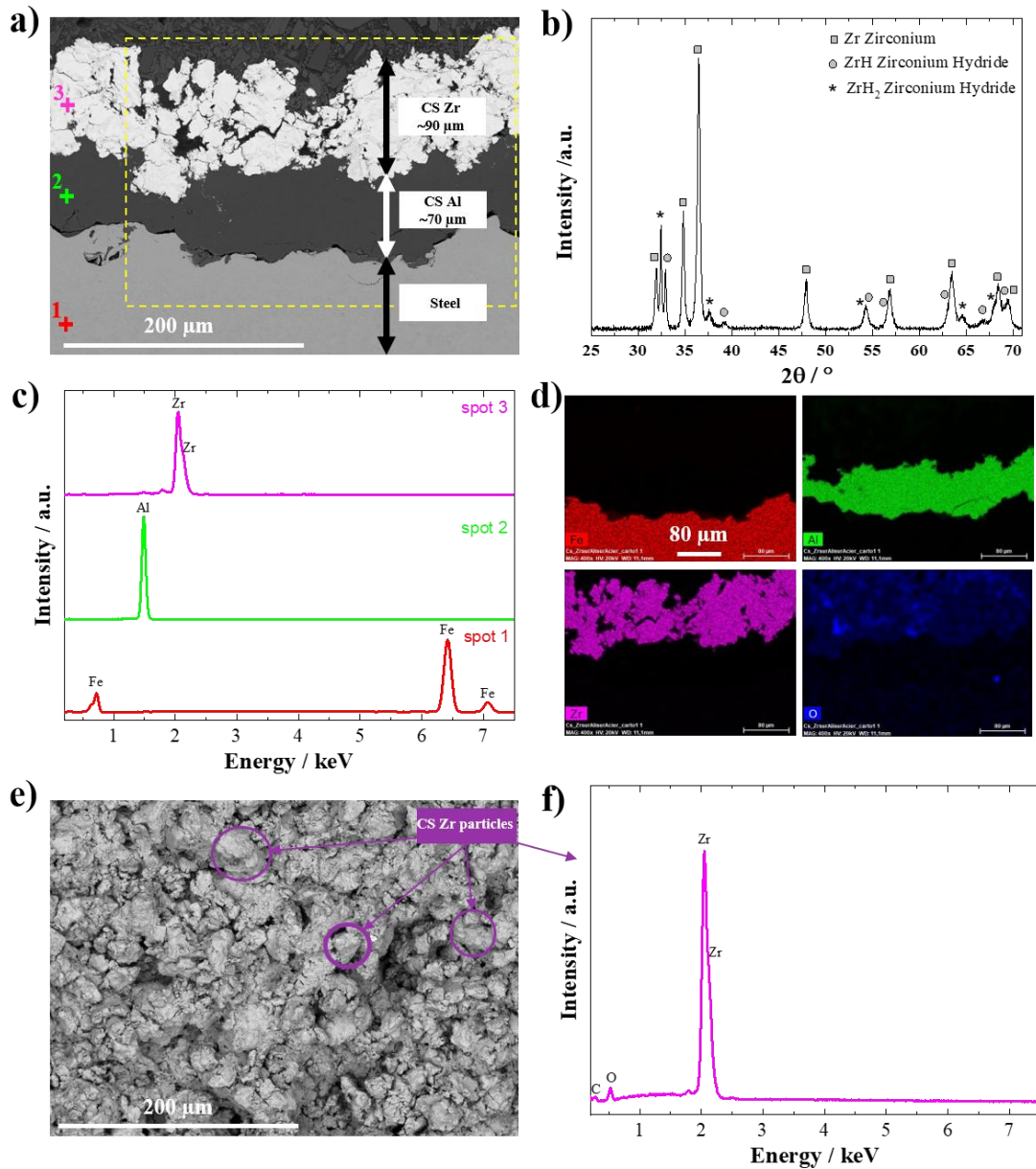


Figure 3: a) Cross-sectional SEM micrograph and b) XRD pattern recorded on the Zr / Al metallic multilayer coating cold-sprayed on a steel substrate, and c) the corresponding EDX spectra and d) EDX elemental mappings in Fe, Al, Zr and O. EDX spectra are recorded at locations indicated by the numbered spots in fig. 3a. Boundary of the EDX elemental mapping is defined by the yellow dashed rectangle in fig. 3a. e) Top surface SEM micrograph recorded on the cold-sprayed Zr outer coating and f) the EDX spectrum recorded on the cold-sprayed Zr particles.

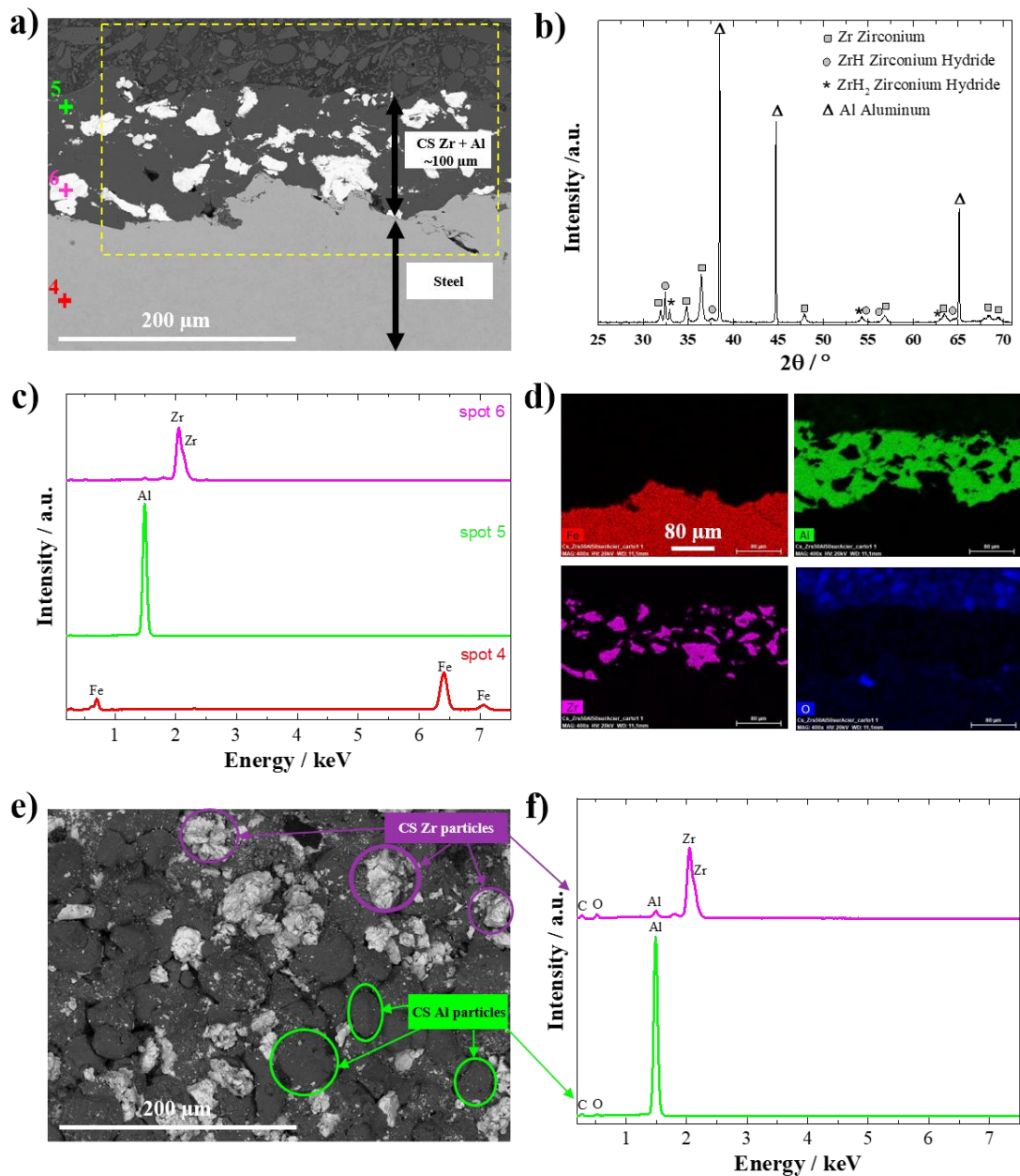


Figure 4: a) Cross-sectional SEM micrograph and b) XRD pattern recorded on the (Zr, Al) metallic composite monolayer coating cold-sprayed on a steel substrate, and the corresponding c) EDX spectra and d) EDX elemental mappings in Fe, Al, Zr and O. EDX spectra are recorded at locations indicated by the numbered spots in fig. 4a. Boundary of the EDX elemental mapping is defined by the yellow dashed rectangle in fig. 4a. e) Top surface SEM micrograph recorded on the cold-sprayed (Zr, Al) composite coating and f) the EDX spectra recorded on the cold-sprayed Zr and Al particles.

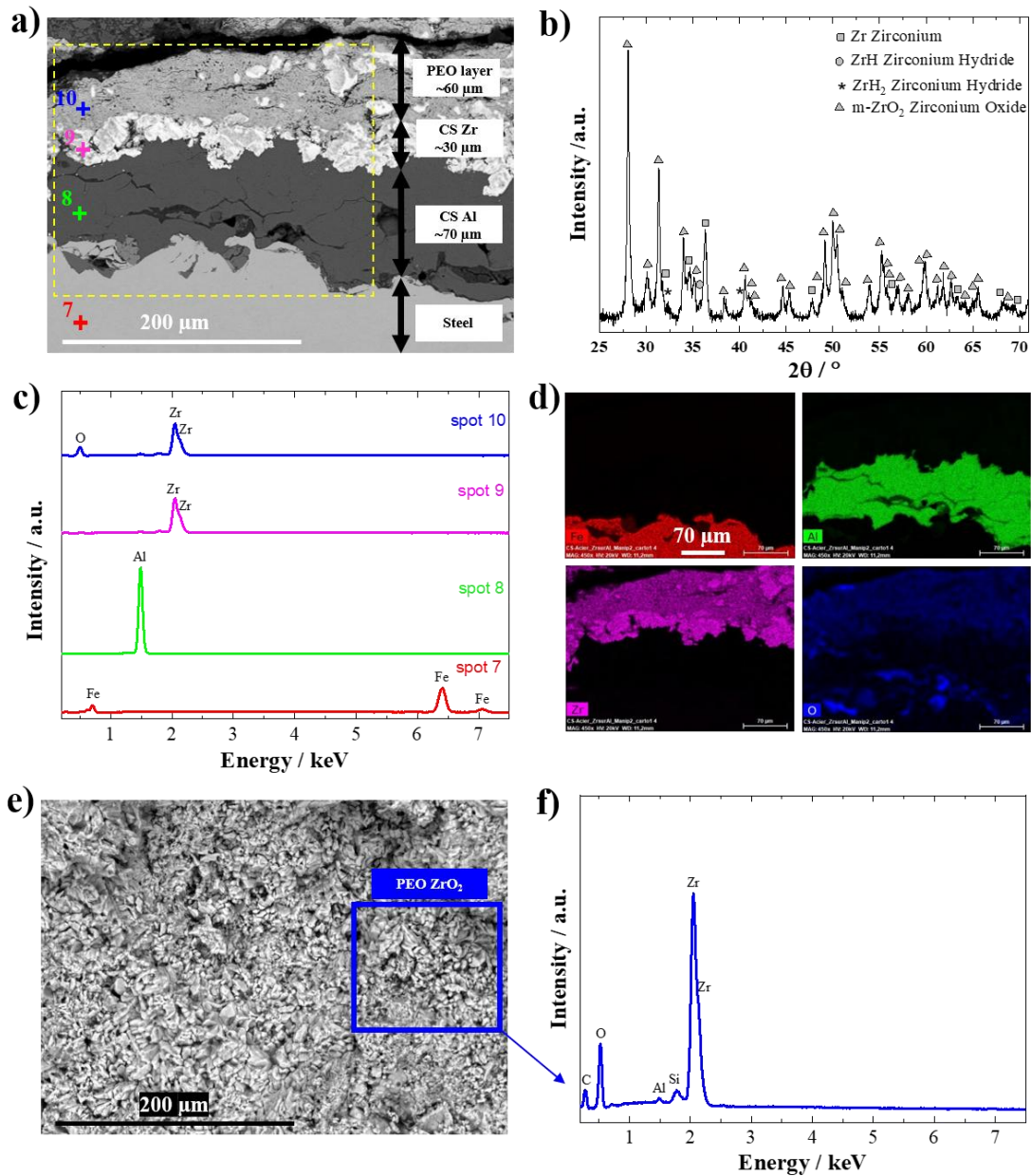


Figure 5: a) Cross-sectional SEM micrograph and b) XRD pattern recorded, after PEO process, on the Zr / Al metallic multilayer coating cold-sprayed on a steel substrate, and the corresponding c) EDX spectra and d) EDX elemental mappings in Fe, Al, Zr and O. EDX spectra are recorded at locations indicated by the numbered spots in fig. 5a. Boundary of the EDX elemental mappings is defined by the yellow dashed rectangle in fig. 5a. e) Top surface SEM micrograph recorded, after PEO process, on the cold-sprayed Zr outer coating and f) the EDX spectrum recorded on the ZrO₂ coating.

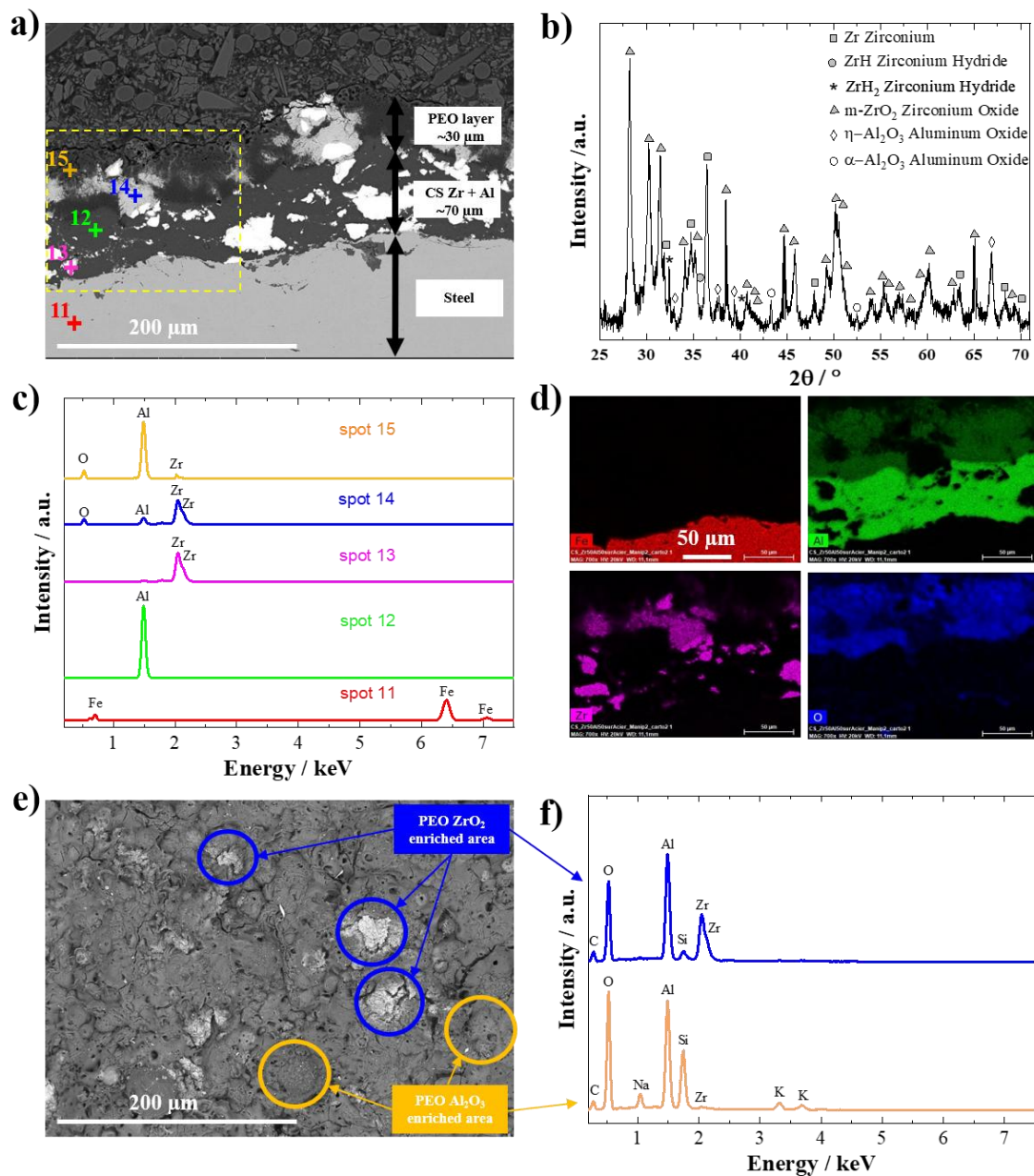


Figure 6: a) Cross-sectional SEM micrograph and b) XRD pattern recorded, after PEO process, on the (Zr, Al) metallic composite monolayer coating cold-sprayed on a steel substrate, and the corresponding c) EDX spectra and d) EDX elemental mappings in Fe, Al, Zr and O. EDX spectra are recorded at locations indicated by the numbered spots in fig. 6a. Boundary of the EDX elemental mapping is defined by the yellow dashed rectangle in fig. 6a. e) Top surface SEM micrograph recorded, after PEO process, on the cold-sprayed (Zr, Al) composite coating and f) the EDX spectra recorded on the ZrO₂ and Al₂O₃ enriched area.